Quadratic detection-based millimeter-wave MMIC for wireless communication and localization

Christophe Loyez, Michael Bocquet, Kamel Haddadi

Quadratic Detection-Based Millimeter-Wave MMIC for Wireless Communication and Localization

Christophe Loyez, Michael Bocquet, Kamel Haddadi

Institut d'Electronique, de Microélectronique et de Nanotechnologies (IEMN), Université de Lille, CNRS, Université Polytechnique Hauts-de-France, UMR 8520 – IEMN, F-59000 Lille, France.

(Corresponding author : kamel.haddadi@univ-lille.fr)

***Abstract* — This paper presents a multi-functional topology of a monolithic microwave monolithic integrated circuit (MMIC) capable of performing both wireless communications and geolocation devices. The architecture of this MMIC allows several RF functionalities such as conventional frequency heterodyning for high-speed IQ modulation. In addition, the device can be configured in quadratic sensing mode to achieve optimal power added efficiency (PAE). The topology developed in the 65 nm FDSOI CMOS technology enables wide frequency band of operation and combines vector accuracy for high data rates and phase state determination. The results presented concern QPSK and 16QAM modulation schemes at data rates up to 2 Gbps as well as essential geolocation measurements such as Time Difference of Arrival (TDoA) and Angle of Arrival (AoA). The expected performance in terms of location accuracy is also presented.**

***Index Terms* — Monolithic microwave integrated circuit (MMIC); IQ modulation; Millimeter wave; Time Difference of arrival (TDoA); Angle of arrival (AoA).**

I. Introduction

With the new generations of wireless communication systems involving in particular beamforming techniques [1], the need for geolocation is becoming more and more important. In addition, the need for ever-increasing data rates is conducive to the increase in frequency. Thus, RF systems operating in the millimeter-wave range are expected to be part of the next generation of post-5G communications systems [2]. In this way, RF front-ends are expected to become more versatile and to be able to perform geolocation and communication functions on the same chip. In this context, this work shows a vector topology of MMICs that meets the requirements of both geolocation and wireless communication. In a first part, the general topology is detailed as well as the different possible modes of use. The experimental results of the IQ modulation mode of this MMIC are presented for data rates up to 2 Gbps. In a second part, the quadratic detection mode is highlighted with experimental results presenting the performance of the MMIC in V-band. Finally, the third part deals with the behavioral model of a geolocation system based on this MMIC in a TDoA / AoA data fusion context.

II. MMIC topology

The overall architecture presented hereafter is based on the topology of a direct-conversion IQ modulator. The design requires overcoming several limitations related to the fact that the different local oscillator (LO) and RF microwave inputs both operate in the same millimeter wave range. It is therefore essential to be able to contain the cross-talks between the different channels. This is made possible in particular by the play of phase shifts. From a global point of view, this architecture includes one differential LO input, one RF port configurable in input or output mode, and four baseband ports corresponding to the differential in-phase I+, I- and quadrature Q+, Q- signals. By adjusting the phase shifts, the leakage of the signal provided by the local oscillator (LO signal) is cancelled and the baseband I and Q channels are balanced. For this purpose, this vector topology of MMIC is illustrated in Figure 1. The phase shifts, provided by differential LO inputs together with quarter-wavelength λg/4 transmission lines (TL), are induced on the four different baseband ports are 0°, 90°, 180° and 270° respectively. The differential signal of the 60 GHz LO is distributed over the 4 baseband channels using two active power splitters. These provide the necessary isolation (> 25 dB) be-tween the different baseband channels and amplify the signals distributed in this way.

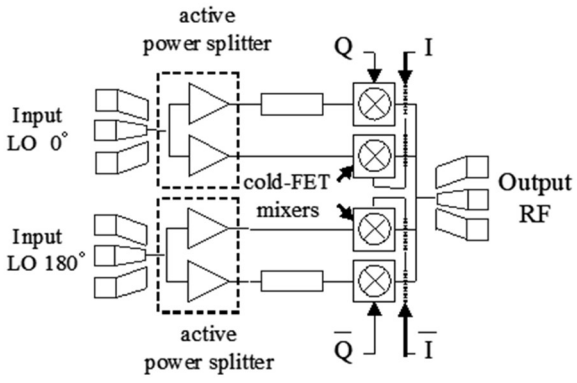

Fig. 1. Synoptic of the overall MMIC topology

The IQ modulation mode corresponds to the case where the order of magnitude of the LO signal power is close to the milliwatt. This mode corresponds to the conventional heterodyne architecture to address IQ modulation [3]. In this case, each n-MOS mixer is simultaneously pumped by each of the phase-shifted contributions of the LO signal and can be considered, as a first approximation, as a switch in the ON or OFF state. This hashing in the time domain induces the frequency transposition of the desired incident signal. This frequency transposition can be up-conversion or down-conversion. By adjustments of the phase-shifts, when I+, I- and Q+, Q- signals are configured as input signals, the MMIC allows to realize the functionality of a vector modulator. This MMIC functionality is tested by considering a high throughput 16QAM modulation scheme. The modulation signals are injected at the I+, I- and Q+, Q- inputs at rates of several Gigabits per second. In order to be able to quantify the vector accuracy of this operation, the RF signal resulting from this vector modulation is frequency down-converted using an external mixer. This RF signal is then converted into an intermediate frequency signal (IF = 1.5 GHz) which is then sampled using a fast digitizing scope.

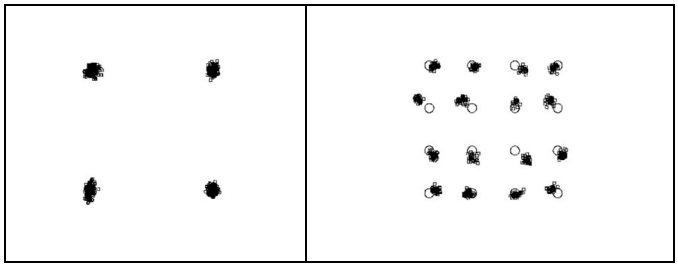

Fig. 2. Measured constellation diagram at the test frequency 61 GHz – (a) QPSK @ 1 Gbps (b) 16QAM @ 2 Gbps

The vector accuracy of the modulation performed by the MMIC is then evaluated us-ing vector signal analysis software. The constellation diagram of the analyzed signal is shown in Figure 2. Table I summarizes the extracted error vector magnitude (EVM) measured for the 16QAM modulation scheme for increasing data rates up to 2 Gbps.

Table 1. Experimental EVM values (%) for QPSK & 16QAM modulated signals at the MMIC RF output (PRF = Pout 1DBc)

Data rate (Mbps)	500	1 000	1500	2000
QPSK	3.8 %	4.8 %	5.7 %	6.6 %
16QAM	6.8 %	9.7 %	10.6 %	11.2 %

These test results are obtained when the power of the output RF signal has been chosen equal to the compression point at 1dB (PRF = Pout 1DBc = -6 dBm). We note a satisfactory concordance between our behavioral model and the experimental validation. The disparities observed are caused by the test bench, in particular the non-linearities of the external mixer and the bandwidth of the cables. The phase-shift / amplitude balance of the different channels I+, I- and Q+, Q- is validated by these results since the EVM is in the range of 10% for a power consumption of 24 mW.

III. QUADRATIC DETECTION MODE

For this MMIC, another operating mode is possible by means of quadratic detection: in this mode, the incident signals, LO and RF, both have a microwave power not exceeding -20 dBm. Each phase-shifted contribution of the LO signal is incident at one end of one of the four passive mixers. The other ends of the mixer receive a portion of the other RF signal. The signals are then combined directly within the common source N-MOS transistor without the need for an additional power splitter or coupler, thus avoiding an increase in overall space requirements. As a result, this configuration is typical of the so-called six-port topology [4]-[23]. In this operating mode, the potentials VDo and VGo of the transistors composing each mixer are used to extract the relevant information. In fact, the VDG voltage (VDG = VDo – VGo), measured in DC operation when RF and LO signals are applied, then corresponds to the quadratic sensing voltage.

Considering the respective expressions for the signals LO and RF, the detected voltage can be expressed as follows:

$$s_{LO}(t) = A_{LO} e^{j(\omega_{LO} t + \varphi_{LO})}$$

$$s_{RF}(t) = A_{RF} e^{j(\omega_{RF} t + \varphi_{RF})}$$

$$\begin{aligned} V_{DG} &= \gamma |s_{LO}(t) - s_{RF}(t)|^2 \\ &= \gamma (A_{LO}^2 + A_{RF}^2 - A_{LO}.A_{RF}.\cos[(\omega_{RF} t + \varphi_{RF}) - \\ &\quad (\omega_{LO} t + \varphi_{LO})]) \end{aligned} \tag{2}$$

The factor γ quantifies the sensitivity of each n-MOS mixer. For each of the four contributions I^+, I^- and Q^+, Q^-, the first of the two terms in relation (2) are rectified signals, while the last contains, in sinusoidal form, the signal of interest (amplitude and phase-shift).

In order to evaluate the MMIC operating in quadratic detection, the measurement bench comprising two frequency generators (Keysight® E8257D PSG) used to generate LO and RF millimeter wave signals is modified. These generators are slaved on the same 10 MHz reference signal. The signals thus delivered are therefore frequency-synchronous. In addition, the phase-shift and attenuation between the two waveforms are perfectly controlled. The measurement frequency is 60 GHz and the power at the input of the MMIC varies between -24 dBm and -19 dBm for the LO signal and between -44 dBm and -24 dBm for the RF signal.

For each combination of phase-shift and power, the detected

voltages V_{det} relative to channels I^+, I^- and Q^+, Q^- are recorded. Phase -shift steps of 10° are considered in the range 0° – 360°. The average error is calculated from the measured V_{det} voltages in each case. In the above-mentioned RF power range, the mean error is determined for LO power values below -20 dBm.

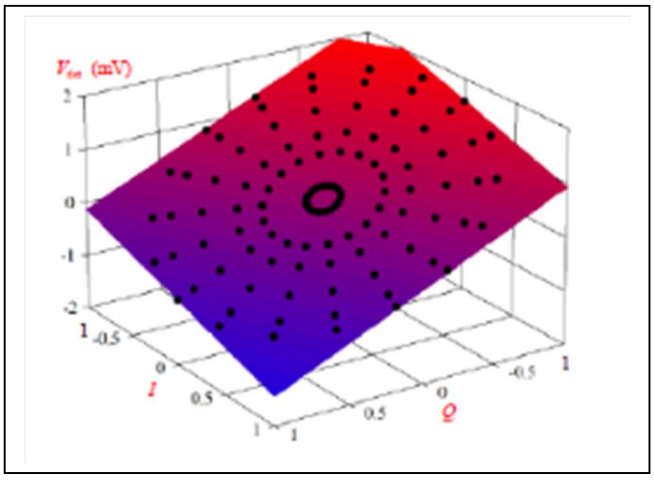

Fig. 3. 3-dimensional fitting of the detected voltage Vdet as a function of I and Q ; F=60 GHz

In this case, the mean error is determined experimentally to be in the order of 1.3%. Under these conditions, we measure a relatively constant sensitivity for all frequencies between 50 GHz and 70 GHz. Typically, this sensitivity is of the order of 1.6 mV/µW at 60 GHz while the mixers are not polarized (zero-bias).

IV. AoA and TDoA determination based on quadratic detection mode

We consider a configuration for which this vector topology allows the detection of both the Time Difference of Arrival (TDoA) and the Angle of Arrival (AoA) by quadratic detection. described Figure 4, the global system topology involving the MMIC mainly comprises two patch antennas followed by two low noise amplifiers. The power gain and the noise figure are respectively equal to 42 dB and 6 dB. The LO (differential) and RF (single-ended) signals received and amplified are collected by the MMIC.

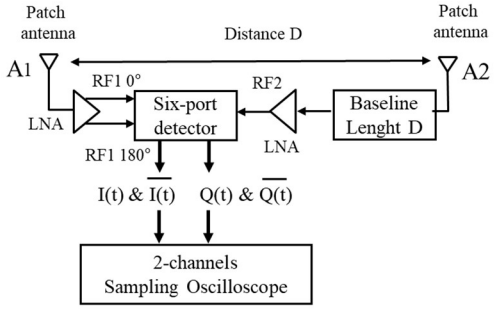

Fig. 4. MMIC-based receiver for AoA / TDoA configuration

An essential parameter is the distance d between the antennas that need to be set to the free-space half-wavelength (λ/2) for AoA measurement. This distance requires to be of several free-space wavelengths for TDoA and closely depend on the RF signal bandwidth. As a function of the distance d between the antennas A1 and A2 and the waveform signal emitted by the transmitter, the vector topology described above can estimate the AoA as well as the TDoA.

When d = λ/2, the phase difference Δφ = π.sin(AoA) can be extracted from the differential I(t) and Q(t) signals.

The root mean square error (RMSE) associated with the AOA estimate depends on both the received signal power and the noise level. From the behavioral model based on Circuit Envelope simulations, the evolution of the RMSE is established in Figure 5 as a function of the signal-to-noise ratio (SNR) for received power values of -19 dBm and -24 dBm at the inputs of the MMIC.

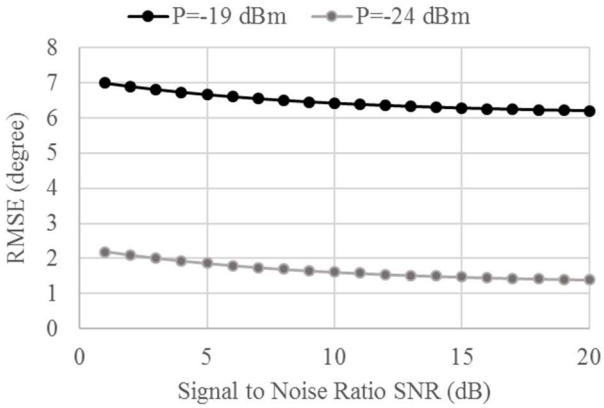

Fig. 5. AoA RMSE at the test frequency 61 GHz

This model thus allows to establish a link between the AoA accuracy and the received power as well as the SNR. In the same way, the accuracy of TDOA is evaluated. The sensitivity of the MMIC does not induce any significant degradation on the TDOA measurement. The sources of errors are mainly caused by the acquisition method (digitizing scope) and the extraction method (autocorrelation). With this operating mode, time resolution and RMSE are strongly dependent on the sampling frequency Indeed, the spatial RMSE related to the TDOA is expressed by:

$$\sigma_{TDOA} = \frac{2.c}{f_s.\sqrt{SNR}} \quad (3)$$

Based on this expression, Figure 11 shows the evolution of the spatial RMSE (expressed in centimeters) as a function of the SNR for a sampling rate of 10 GSa/s. Typically the inaccuracy of the estimated TDOA is reflected in the distance domain by a deviation between 7 and 28 centimeters as depicted by Fig. 6.

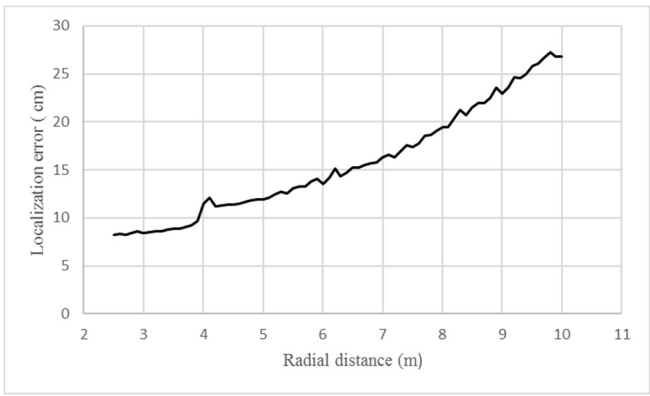

Fig. 6. Evolution of the localization error as a function of the radial distance

Based on previous measurements and simulations, a model of the MMIC characteristics is built on Matlab, integrating its frequency and non-linear imperfections in the vector domain. On the basis of this model, a receiver configuration as described in Figure 4 integrating this MMIC is considered to detect both TDoA and AoA. As previously mentioned, the distance between the antennas is a crucial parameter. In the case of TDoA, this distance is fixed at 5 cm while the value of 3 mm (λ/2) is used for the estimation of the AoA. Figure 7 compares the performance of three location systems for which MMIC is at the center of their topology: one includes two synchronous receivers operating only in TDoA mode, the second is similar to the first but the operation of both receivers is exclusively focused on AoA. The third localization system consists of a single receiver allowing the two modes to be combined and TDoA/AoA merged.

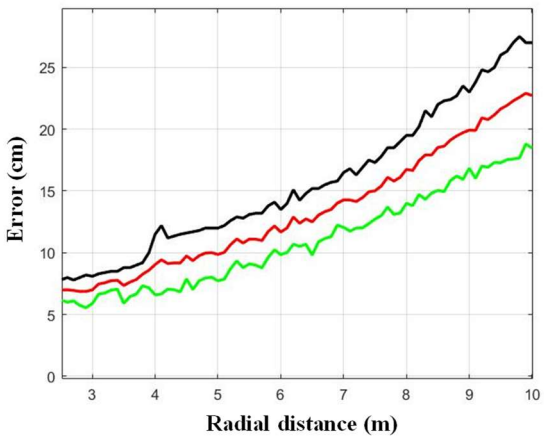

Fig. 7. Location errors (in centimeters) versus radial distance (in meters) for a low azimuth angle in three configurations: TDoA/TDoA and AoA/AoA (where 2 receivers are spaced 1 m apart) and a TDoA/AoA combination involving a single receiver.

Red line: Fusion AoA/AoA; Black line: Fusion TDoA/TDoA; Green line: Fusion AoA/TDoA

In order to validate the performance by a statistical approach, we considered more than one hundred positions with radial distances of up to 10 meters in an intramural environment. In the case of low azimuth angle, the maximum error obtained is 27.6 centimeters in the case of TDoA/TDoA. This maximum error is reduced to 23 centimeters in the case of AoA compared to 18 centimeters in the case of TDoA/AoA data fusion. One can note that these performances fully meet the specifications generally adopted for indoor geolocation systems [24].

V. Conclusion

This versatile topology provides attractive performance within a single MMIC to deliver a variety of features essential to the next generation of radio frequency devices. Adopting a broadband frequency behavior and a balanced compromise between linearity and power consumption, the experimentally verified vector accuracy in both IQ modulation and quadratic detection makes this RF architecture an excellent candidate to meet the requirements of 5G and beyond.

References

[1] W. Miao, C. Luo, G. Min and Z. Zhao, "Lightweight 3-D Beamforming Design in 5G UAV Broadcasting Communications," *IEEE Transactions on Broadcasting*, vol. 66, no. 2, pp. 515-524, June 2020.

[2] W. Hong et al., "The Role of Millimeter-Wave Technologies in 5G/6G Wireless Communications," *IEEE Journal of Microwaves*, vol. 1, no. 1, pp. 101-122, winter 2021.

[3] W. Zhou, L. Zhao, J. Zhang and K. Wang, "Four Sub-Channel Single Sideband Generation of Vector mm-Wave Based on an I/Q Modulator," *IEEE Photonics Journal*, vol. 11, no. 4, pp. 1-9, Aug. 2019.

[4] A. Koelpin, F. Lurz, S. Linz, S. Mann, C. Will and S. Lindner, "Six-port based interferometry for precise radar and sensing applications", *Sensors*, vol. 16, no. 1556, pp. 1–26, Sept. 2016.

[5] K. Haddadi and T. Lasri, "Formulation for complete and accurate calibration of six-port reflectometers", *IEEE Trans. Microw. Theory Tech.*, vol. 60, no. 3, pp. 574–581, March 2012.

[6] K. Haddadi, MM.Wang, D. Glay, and T. Lasri, "Performance of a Compact Dual Six-Port Millimeter-Wave Network Analyzer", *IEEE Trans. Instrum. Meas.*, vol. 60, no. 9, pp. 3207–3213, Sept. 2011.

[7] K. Haddadi and C. Loyez, "65 nm SOI CMOS 60 GHz passive mixer for six-port technology," 2016 IEEE Topical Conference on Wireless Sensors and Sensor Networks (WiSNet), Austin, TX, 2016, pp. 52-55.

[8] K. Haddadi, H. El Aabbaoui, B. Gorisse, D. Glay, N. Rolland and T. Lasri, "A fully InP monolithic integrated millimeter-wave reflectometer," *36th European Microwave Conference*, pp. 703-706, 2006.

[9] M. Wang, K. Haddadi, O. Benzaim, D. Glay, and T. Lasri, "Six-port based near-field millimeter-wave microscope using a slit scanning probe," *IEEE Int. Conf. on Electromagnetic Near-field Characterization & Imaging*, pp. 17–22, Taipei, Taiwan, June 2009.

[10] K. Haddadi, M. Wang, D. Glay ad T. Lasri, "A new range finder based on a four-port junction, *IEEE Sensors Journal*, vol. 9, no 6, pp. 697-698, 2009.

[11] K. Haddadi, M. Wang, D. Glay and T. Lasri, "Free-space microwave moisture content evaluation by means of a low-cost four-port based

reflectometer,". *8th International Conference on Electromagnetic Wave Interaction with Water and Moist Substances, ISEMA,* pp. 63-70, 2009.

[12] K. Haddadi, MM.Wang, O. Benzaim, D. Glay, and T. Lasri, "Contactless microwave technique based on a spread-loss model for dielectric materials haracterization," *IEEE Microw. Wireless Compon. Lett.,* vol. 19, no. 1, pp. 33–35, Jan. 2009.

[13] K. Haddadi, M. Wang, D. Glay and T. Lasri, "A 60 GHz six-port distance measurement system with sub-millimeter accuracy," *IEEE Microw. Wireless Compon. Lett*, vol. 19, no. 10, pp. 644-646, 2009.

[14] K. Haddadi, D. Glay and T. Lasri, "A 60 GHz scanning near-field microscope with high spatial resolution sub-surface imaging *IEEE Microw. Wireless Compon. Lett.*, vol. 21, no. 11, pp. 625-627, 2011.

[15] K. Haddadi, M. Wang, D. Glay ad T. Lasri, "60-GHz near-field six-port microscope using a scanning slit probe for subsurface sensing," *IEEE Sensors Journal*, vol. 12, no. 8, pp. 2575-2576, 2012.

[16] K. Haddadi, and T. Lasri, "V-band two-tone continuous wave radar operating in monostatic/bistatic mode", *9th European Radar Conference (EuRAD)*, pp. 266-269, 2012.

[17] K. Haddadi, and T. Lasri, "The muti-port technology for microwave sensing applications," *IEEE MTT-S International Microwave Symposium Digest*, pp. 1-3, 2012.

[18] K. Haddadi, and T. Lasri, "Six-port-based compact and low-cost near-field 35 GHz microscopy platform for non-destructive evaluation.," *NDT & E International*, vol. 55, pp. 102-108, 2013.

[19] K. Haddadi, and T. Lasri, "CW radar for monitoring water-to-cellular concrete," *44th European Microwave Conference (EuMC),* pp. 1832-1835, 2014.

[20] K. Haddadi, and T. Lasri, "Six-port technology for millimeter-wave radar and imaging applications", *IEEE WiSNet Conf.,* pp. 1-3, 2014.

[21] A. El Fellahi, K. Haddadi, D. Glay ad T. Lasri, "Multiport reflectometer based on subtractive mixing," *IEEE Sensors Journal*, vol. 15, no. 9, pp. 4729-4730, 2015.

[22] K. Haddadi and C. Loyez, "Millimeter-wave six-port IQ demodulator in 65 nm SOI CMOS technology," *IEEE Instrumentation and Measurement Technology Conference Proceedings (I2MTC)*, pp. 1-5, 2016.

[23] K. Haddadi, C. Loyez,L. Clavier, D. Pomorski and S. Lallemand, "Six-port reflectometer in WR15 metallic waveguide for free-space sensing applications," *IEEE WiSNet Conf.,* pp. 80-83, 2018.

[24] E. O'Lone, H. S. Dhillon and R. M. Buehrer, "Single-Anchor Localizability in 5G Millimeter Wave Networks," *IEEE Wireless Communications Letters*, vol. 9, no. 1, pp. 65-69, Jan. 2020